Highly Viscoelastic, Stretchable, Conductive, and Self-Healing Strain Sensors based on Cellulose Nanofibers-Reinforced Polyacrylic Acid Hydrogel

Yue Jiao
Nanjing Forestry University
Kaiyue Lu
Nanjing Forestry University
Ya Lu
Nanjing Forestry University
Yiying Yue
Nanjing Forestry University
Xinwu Xu
Nanjing Forestry University
Huining Xiao
University of New Brunswick
Jian Li
Northeast Forestry University
Jingquan Han (hjq@njfu.edu.cn)
Nanjing Forestry University https://orcid.org/0000-0002-1306-5431

Research Article

Keywords: Cellulose Nanofibers, Mechanical Property, Self-Healing, Strain Sensing

Posted Date: February 23rd, 2021

DOI: https://doi.org/10.21203/rs.3.rs-231511/v1

Version of Record: A version of this preprint was published at Cellulose on March 9th, 2021. See the published version at https://doi.org/10.1007/s10570-021-03782-1.

Abstract

Conductive and self-healing hydrogels are among the emerging materials that mimic the human skin and are important due to their probable prospects in soft robots and wearable electronics. However, the mechanical properties of the hydrogel matrix limit their applications. In this study, we developed a physicochemically dual cross-linked chemically modified-cellulose nanofibers-carbon nanotubes/polyacrylic acid (TOCNF-CNTs/PAA) hydrogel. The TOCNFs acted both as a nanofiller and dispersant to increase the mechanical strength of the PAA matrix and break the agglomerates of the CNTs. The final self-healing and conductive TOCNF-CNTs/PAA-0.7 (mass ratio of CNTs to AA) hydrogel with a uniform texture exhibited highly intrinsic stretchability (breaking elongation to ca. 850%), enhanced tensile properties (ca. 59kPa), ideal conductivity (ca. 2.88S·m^{-1}) and pressure sensitivity. Besides, the composite hydrogels achieved up to approximately 98.36% and 99.99% self-healing efficiency for mechanical and electrical properties, respectively, without any external stimuli. Therefore, the as-designed multi-functional self-healing hydrogels, combined with stretching, sensitivity, and repeatability, possess the ability to monitor human activity and develop multifunctional, advanced, and commercial products such as wearable strain sensors, health monitors, and smart robots.

Introduction

Nature has provided endless inspirations to promote biomimetic synthetic materials (Dai et al. 2019; Li et al. 2019; Liu et al. 2017). In addition to being elastic, flexible, and self-healing, human skin also has unique mechanical and sensory properties. In the past few years, the electronic skin (E-skin) has received significant attention as an excellent candidate for human skin (Wang et al. 2015; Yang et al. 2019a). The E-skin can mimic the human skin to detect current response by converting environmental stimuli into an electrical signal (such as strain, pressure, temperature, etc.), and this holds great promise in soft robotics, sensors, and artificial intelligence (Dong et al. 2018; Liu et al. 2018b; Schwartz et al. 2013; Yang et al. 2019b). Nevertheless, there remains a tremendous challenge in the synthesis of E-skin materials that combine both adaptable stretch-ability and exceptional self-healing ability. Notably, self-healing hydrogel-based sensors are expected to assemble the E-skin based on high mechanical strength and conductivity (Liu et al. 2018a; Xia et al. 2019; Xu et al. 2019). Recently, research has focused on polyacrylic acid (PAA) hydrogel as a raw material for producing autonomous self-healing materials (Wei et al. 2013). It is worth noting that PAA contains numerous carboxyl groups, which are crucial for the design of the self-healing hydrogels. Huang et al. (Huang et al. 2015) reported a PAA electrolyte gel with self-healing ability, which can address the damage problems of a supercapacitor during practical applications due to the intrinsic self-healing ability and high stretch-ability. Anjum et al. (Anjum et al. 2017) explored the superabsorbent PAA hydrogels cross-linked with trivalent aluminum ions, which exhibited an excellent self-healing efficiency. On the other hand, Wang et al. (Wang et al. 2018a) reported a ternary polymer material comprising of PAA, phytic acid (PA) and polyaniline (PANI) with a high stretch-ability, controllable conductivity, and good self-healing properties. The PAA/PA/PANI hydrogels could be used in the production of strain sensors which depended on their strain sensibility. However, self-healing PAA

hydrogels have some limitations due to poor mechanical properties and absence of electrical conductivity, which restrict their practical applications.

In general, the mainstream strategy for reaching a sufficiently high electrical conductivity for hydrogels is to incorporate conductive materials such as graphene (GN), reduced graphene oxide (rGO), carbon nanotubes (CNTs), or conductive polymers (Hu et al. 2019; Wan et al. 2019; Wan and Li 2016). However, GN, rGO, and CNTs are inclined towards self-aggregation and maldistribution because of their inherent disadvantages (Ma et al. 2010). Previous studies have reported that one dispersion strategy is surface oxidation or chemical grafting in an aqueous medium to introduce repulsive interactions or steric hindrance for colloidal stability (Gao et al. 2016a; Massoumi et al. 2014). However, this strategy leads to low adhesion and disrupts the electronic structure, thereby causing a reduction in the conductivity. Consequently, another approach based on non-covalent functionalization has been suggested to overcome the above problems and obtain highly conductive elastomeric hydrogels. Conductive materials are dispersed in an aqueous medium via ultrasonic treatment to form long-standing stably dispersed colloidal with the use of a nanofiller (Krause et al. 2010; Lu et al. 2018; Tang et al. 2011). One study prepared cellulose nanofibers using 2,2,6,6-tetramethylpiperidine-1-oxyl (TEMPO)-oxidized cellulose nanofibrils (TOCNFs), which are attractive as reinforcing fillers due to their high aspect ratio, decent Young's modulus, and a chemically modifiable surface (Koga et al. 2013). Moreover, the electrostatic repellent interaction between the negatively charged carboxylate ions of the carboxyl groups on the TOCNFs surfaces allows them to have an individual uniform dispersion in water (Olivier et al. 2012). For example, Han et al. (Han et al. 2019) developed a type of multifunctional electro-conductive hydrogels based on a polyvinyl alcohol-borax (PVAB) hydrogel and carbon nanotube-cellulose nanofiber (CNT-CNF) nanohybrids. Nanocellulose was used as a biotemplate and dispersant to carry CNTs to form CNT-CNF hybrids with good dispersibility, which not only enhanced the viscoelasticity and mechanical toughness, but also endowed high electrical conductivity and stability to hydrogels. Furthermore, several studies have used TOCNFs as nanofillers to reinforce the matrix materials. For instance, Fujisawa et al. (Fujisawa et al. 2012) fabricated TOCNF/polystyrene nanocomposite films, which exhibited increased tensile strengths and elastic moduli by the addition of TOCNF. Besides, the TOCNF/polystyrene films displayed high optical transparencies and thermal dimensional stabilities. The study further discussed the impact of the TOCNF content on performance. Chen et al. (Chen et al. 2019) reported stretchable and self-healing TOCNF/PAA-PPy hybrid hydrogels, which displayed reinforced mechanical performances, electroconductivity, and self-healing properties. Besides, the high aspect ratio and decent Young's modulus of the TOCNFs benefited network formation, stress transfer, and increased the stiffness of composite materials.

In this study, we focused on a highly viscoelastic, stretchable, conductive, and self-healing hydrogel for application in strain sensing. The study used simple in-situ polymerization to chemically crosslink PAA chains and form a hydrogel network, which could hold the mechanical structure of the hydrogel. The TOCNFs acted as both nanofiller and dispersant due to carboxyl groups and hydroxy groups on it's surface. Formulation of the TOCNF-CNTs/PAA hydrogels involved dispersing TOCNF-CNTs complexes in

the PAA matrix and using Fe^{3+} as an ion crosslinking agent. The introduction of Fe^{3+} ions in the PAA hydrogels caused strong dynamic reversible non-covalent crosslinking through metal coordination bonds. The mechanical properties of the hydrogel were further enhanced by hydrogen-bonds between the TOCNFs and the PAA chain. Specifically, the carboxyl groups on the TOCNFs also formed metal coordination with Fe^{3+} to increase the crosslink density. Moreover, the addition of CNTs also increased the electrical conductivity of the hydrogels. The obtained hydrogels displayed reinforced mechanical strength, viscoelasticity, stretch-ability, conductivity, and self-healing ability, due to the synergistic effects of PAA, TOCNFs, and CNTs. Therefore, the TOCNF-CNTs/PAA hybrid hydrogels are expected to expend the application of hydrogels in strain sensors, wearable electronics, health monitors, and smart robots.

Materials And Methods

Materials

Bleached wood pulp (BWP) which is the cellulose source, was purchased from Nippon Paper Chemicals (Tokyo, Japan), purified and vacuum dried before use. CNTs were acquired from Chengdu Organic Chemicals Co., Ltd. TEMPO, while sodium hypochlorite (NaClO), sodium bromide (NaBr), acrylic acid (AA), N, N'-methylene bisacrylamide (MBA), aniline monomer (ANI), iron chloride hexahydrate, and ammonium persulphate (APS) were procured from Sigma-Aldrich.

Preparation of TOCNFs

Cellulose fibers were modified using the TEMPO/NaBr/NaClO system at pH 10 and NaClO at 15mmol g^{-1} of cellulose weight, following a previously reported protocol (Isogai et al. 2011; Saito et al. 2006). In a typical process, 2g of dried BWP were suspended in deionized water containing 0.033g of TEMPO and 0.33g NaBr, followed by homogenization by continuous stirring. Subsequently, the oxidation process was caused by adding the NaClO solution slowly into the slurry at ambient temperature. This was followed by dripping 0.5M NaOH to adjust the pH (10) of the mixture under stirring. The oxidation process was then terminated using excess ethanol. Finally, the products were collected by repeated filtration at a PH of 7, and then freeze-dried for further experiments.

Fabrication of the TOCNF/CNTs-PAA hydrogels

The TOCNF/PAA-CNTs hydrogels were fabricated using the following synthesis process. Firstly, the preprocessed cellulose was sonicated in distilled water to form a 0.8wt% homogeneous aqueous suspension, and the desired number of CNTs was mixed with the suspension. The mixture was ultrasonicated for 30 min using sonifier (Scientz Technology, JY99-IID900 W/20 kHz) to obtain an aqueous TOCNF/CNTs mixture. Meanwhile, 6g of the AA monomer, 0.03g of MBA, and 0.2g of $FeCl_3 \cdot 6H_2O$ were dissolved in 24mL unionized water and treated with bubbling N_2 gas to maintain an anaerobic condition. This was followed by the addition of 15g of the TOCNF-CNTs mixture into the above precursor aqueous solution and then stirred to obtain a uniform mixture. APS was employed as an initiator of the polymerization reaction and proceeded at 40°C for 36 h. The above processes were then

repeated using the TOCNF-CNTs mixed solution with a higher CNTs proportion (i.e., 0.3, 0.5, 0.7, and 1.0wt% mass ratio of CNTs to AA) and the resultant TOCNF-CNTs/PAA hybrid hydrogels were marked as TOCNF-CNTs/PAA-0.3, 0.5, 0.7, and 1.0, respectively (as illustrated in Table S1, Supporting Information). Finally, the obtained hydrogels were successively rinsed with distilled water to remove the extra AA monomer and ions. Pure PAA and TOCNF/PAA hydrogels were synthesized using an identical procedure but without the addition of TOCNFs and CNTs.

Characterization

Field-emission scanning electron microscope (FE-SEM, S-4860, HITACHI, Japan) and Transmission electron microscope (TEM, JEM-1400, JEOL Ltd., Japan) were used for morphological observations. Fourier transforms infrared (FTIR) spectra were recorded on an FTIR instrument (Nicolet iS10, USA) using a range of 500-4000cm^{-1} with a resolution of 4cm^{-1}. Mechanical testing was performed on a universal tensile tester (TY-8000B, Jiangsu tianyuan test equipment co. LTD) at room temperature. Each sample was tested three times. Cylindrical samples with a length of 40 mm and a diameter of 4 mm were used for tensile tests at a tensile rate of 50 mm min^{-1}. Compression tests were performed on disc type samples with a diameter of 40 mm and a thickness of 10 mm at a speed of 15mm min^{-1}. The rheological properties of the hydrogels were measured using a HAAKE RheoStress 600 rheometer (Thermo Fisher Science). The resistance of the samples was monitored at room temperature using the four-point probe method (RTS-8, Heng Odd, China) and the conductivities ($\sigma = L/(R \cdot S)$) of hydrogels were calculated by the resistance (R), distance between the two electrodes (L) and the cross-sectional area (S). Strain sensing tests were carried out using an electrochemical workstation (CS350, Wuhan CorrTest, China). Details of the test conditions are described in the Supporting Information.

Results And Discussion

Schematic diagram of the preparation of TOCNF-CNTs/PAA

Illustration of the fabrication process of TOCNF/PAA-CNTs is shown in Fig. 1a. Firstly, beached wood pulps were oxidized using the TEMPO system. Certain amounts of -COONa and -OH were then imported into the celluloses, thereby leading to the formation of the TOCNFs. It is worth noting that a stable colloidal suspension of the TOCNFs can be formed for a long-term without any aggregation due to the stabilization of surface anionic charges. The CNTs display a strong orientation for aggregation due to the strong van der Waals force attraction among the CNTs. There could be a strong interaction between CNTs and TOCNFs via hydrogen bonding because of a certain number of functional groups (such as − OH and − COOH) generated during the CNTs synthesis process, thereby leading to co-solubility and well-dispersion of CNTs in the solution. In addition, the carboxylate ions on the surface of TOCNFs were negatively charged, and such negatively charged ions can lead to the electron delocalization in the sp_2 carbon lattice of CNTs, forming a dipole, so that the interaction between TOCNFs and CNTs can be combined together (Koga et al. 2013). Therefore, CNTs were added into the stable aqueous suspension of TOCNFs, followed by ultrasonication to obtain a uniform mixture. Subsequently, the TOCNF-CNTs

complexes were incorporated into the aqueous suspension of the AA monomer, Fe^{3+}, and MBA that were degassed and sonicated using N_2 gas under an ice-water bath. Ultimately, the development of the TOCNF-CNTs/PAA self-healing hydrogels involved both physical and chemical crosslinked networks. The specific mechanism of forming the composite hydrogels is displayed in Fig. 1b. Firstly, the PAA chains were fabricated using covalent bonds with an MBA being used as the crosslinking agent. The chemically cross-linked PAA chains, as a mechanically tough backbone, ensured basic mechanical strength and support to sustain the hydrogel shapes. The introduction of the TOCNF-CNTs complexes increased the mechanical strength and enhanced the structural stability of the matrix due to the formation of physical crosslinking through hydrogen bonding and electrostatic interaction between the TOCNF-CNTs and PAA. Besides, the rapidly reversible self-healing mechanism of the crosslinked polymer chains benefitted from the dynamic ionic bonding between ferric ions and carboxylic groups in the damaged region. Therefore, the free trivalent Fe^{3+} ions provided sufficient dynamic crosslinking sites for metal-ligand bonds between Fe^{3+} and carboxylic groups of TOCNF-CNTs and/or PAA. Previous studies have reported that the hydrogels based on reversible non-covalent bonds possessed satisfactory recyclability and self-healing capabilities (Guo et al. 2016; Wei et al. 2013).

Morphological observations and composition analysis

The obtained TEM images (Fig. 2a-c) revealed that the microstructure and the corresponding right insets display the dispersion of TOCNFs, CNTs, and TOCNF-CNTs complexes in water, respectively. Moreover, the fiber-like TOCNFs were homogeneously dispersed to form a transparent and stable dispersion (inset of Fig. 2a). This could be because the introduced carboxyl groups on the surface of the TOCNFs led to electrostatic repulsion between the TOCNFs after TEMPO-mediated oxidation treatment, thereby promoting the uniform and stable TOCNFs dispersion. The average length and diameter of TOCNFs fibers were a few microns and 4±2 nm, respectively, showing a high aspect ratio. CNTs exhibited hollow tubular structures and huge entanglement morphology due to the van der Waals force (Fig. 2b). According to the manufacturer (Chengdu Organic Chemicals Co., Ltd), the diameter and length of pristine CNTs were in the range of 10–20 nm and 30–100 μm. The obtained digital image in the inset of Fig. 2b shows poor dispersibility of the CNTs in water. On the other hand, Fig. 2c shows that the TOCNFs adsorbed on the CNTs surface were separated into individual nanotubes and no severe agglomeration phenomena occurred after hybridization of the TOCNFs and CNTs. The results demonstrated that the TOCNFs can assist in the dispersion of the CNTs due to the hydrogen bonding and hydrophobic effects between the TOCNFs and CNTs (Yang et al. 2018). Besides, a uniform and stable dispersion of the TOCNF-CNTs was obtained (inset of Fig. 2c). The digital images of the TOCNF/PAA, CNTs/PAA, and TOCNF-CNTs/PAA hydrogel are displayed as shown in Fig. 2d-f, respectively, to further verify that the homogeneous dispersion of the CNTs was assisted by TOCNFs in the PAA matrix. As shown in Fig. 2d, the TOCNF/PAA hydrogels exhibited a smooth surface and uniform texture as well as shape stability. Therefore, the TOCNFs and PAA matrix had good compatibility and was uniformly dispersed in the matrix. However, the CNTs/PAA hydrogel had a collapsed structure and distinct stratification with low mechanical properties, which is manifested by a large number of black aggregates entrapped in the brown-red hydrogel matrix

(Fig. 2e). These results also proved that the incorporation of the TOCNFs increased the mechanical strength of the PAA matrix. The TOCNFs-assisted dispersion of CNTs displayed a favorable homogeneity and stability not only in water but also in the PAA hydrogel matrix. Furthermore, the prepared TOCNF-CNTs/PAA hydrogel possessed excellent dispersibility and outstanding mechanical properties (Fig. 2f). These phenomena further confirmed that the added TOCNFs aided in achieving good dispersion of CNTs, and improved the mechanical strength and structural stability of the hydrogels.

The surface chemical compositions of the samples were investigated using FTIR analysis to further establish the above-mentioned mechanism. The absorption peaks at 3322, 1712, and 1454cm^{-1} in the FTIR spectrum of PAA could be attributed to the absorption of O-H symmetric stretching, C = O stretching, and CH_2 symmetric shearing vibrations, respectively (Fig. 3a) (Varga et al. 2017). For TOCNFs, the peaks at 2900, 1409, and 1027cm^{-1} originated from the C – H stretching, CH_2 in-plane bending, and CH bending vibration, respectively (Yu et al. 2014). The peak at around 1600cm^{-1} can be attributed to the carboxylic groups or the bending vibration of O–H because of the TEMPO-mediated oxidation (Yue et al. 2020). The band at 1625cm^{-1} was vested in the C = O stretching vibration in the carboxylic acid groups, indicating the appearance of the – OH and – COOH in the CNTs (Han et al. 2019). Moreover, the characteristic band at 1569cm^{-1} was associated with the C = C asymmetric stretching vibration of the aromatic rings of sp^2 hybridized carbon, while the band at 1382cm^{-1} was associated with the C – C stretching vibration (Zheng et al. 2020). Figure 3b shows the FTIR spectra of the various hydrogels. The – OH stretching peaks of the TOCNF-PAA and TOCNF-CNTs/PAA hydrogels shifted to a low wavenumber (from 3417 to 3216cm^{-1}) when compared with the PAA hydrogel, implying the formation of hydrogen bonds between PAA and either TOCNFs or TOCNF-CNTs. Notably, the feature band of the TOCNFs at 1600cm^{-1} (carboxylate groups) disappeared, while new vibrational absorption peaks occurred at 1712cm^{-1} (C = O stretching vibration of – COOH) after the formation of TOCNF-PAA or TOCNF-CNTs/PAA hydrogels (Zhang et al. 2017). This alteration can be attributed to the fact that the – COOH was transformed into TOCNF-COONa, which was caused by the selective oxidation of C6 primary hydroxyls of cellulose to C6 carboxylic groups through TEMPO pre-treatment. The peak at 1633 cm^{-1} was attributed to water due to the hydrogels were difficult to be dried completely. The obtained SEM images are shown in Fig. 3c and d display the microstructure of the TOCNF/PAA and TOCNF-CNTs/PAA after the freeze-drying process. It is worth noting that both types of samples exhibited a typical porous structure. The incorporation of the TOCNFs-assisted uniform dispersion of CNTs led to more uniform and intensive physical crosslinking points. Besides, the pore size was reduced after the introduction of CNTs, thereby making closer and compact porous structure (Yang et al. 2018).

Dynamic viscoelasticity

Table 1
Rheological parameters derived from moduli curves

Parameter	Critical strains, γ_c (%)	G'_{max} (kPa)	G'_{∞} (kPa)
PAA	6.9	7.2	11.1
TOCNF/PAA	16.4	16.6	7.6
TOCNF-CNTs/PAA-0.3	11.3	18.0	25.7
TOCNF-CNTs/PAA-0.5	4.6	20.3	28.7
TOCNF-CNTs/PAA-0.7	1.8	25.6	31.7
TOCNF-CNTs/PAA-1.0	3.6	23.6	16.2

The viscoelastic properties (G' and G'') of hydrogels were evaluated using strain sweep and frequency sweep. The obtained plots for G' as a function of γ indicated typical viscoelastic and gel-like properties for all the hydrogels (Fig. 4a) (Kumar et al. 2014). The TOCNF-CNTs/PAA hydrogel exhibited the largest G' value, followed by TOCNF/PAA hydrogel, while the PAA hydrogel had the smallest G' value. These results suggested that the addition of the TOCNFs and CNTs prominently increased the viscoelasticity and stiffness of the PAA hydrogel matrix. The extent of LVR, moduli being independent of the strain amplitude, was demonstrated by small-amplitude oscillatory shear tests. The end of LVR was defined as the critical strain (γ_c), which marked the end of the linear stress-strain relationship (Alias and Mhd Sarbon 2019). All the obtained γ_c values in this study ranged from 1.8–16.4% (Table 1). Altogether, the amplitude strain sweep was maintained in the LVR to avoid the destruction of the structure. Thus, $\gamma = 1.0\%$ was chosen for the subsequent tests. The G' value was remarkably increased from 7.2 (PAA hydrogel) to 16.6 kPa (TOCNF/PAA) (Table 1), demonstrating that the viscoelasticity of the PAA hydrogels was substantially reinforced due to the incorporation effect of the TOCNFs. More physical crosslinking points were formed after the addition of the CNTs, which led to a denser structure in the hydrogel, and thus, it showed a higher modulus. Nevertheless, the G' values of the TOCNF-CNTs/PAA-1.0 hydrogel were significantly decreased because the excessive CNTs caused the aggregation and stress concentration. With increasing strain, there was a more significant reduction in the G' value of the TOCNF-CNTs/PAA hydrogel in contrast to those for the PAA and TOCN/PAA hydrogels, which could be attributed to the increase in the rupture of hydrogen bonds and coordination bonds among the PAA, TOCNFs, and CNTs. The rupture of non-covalent bonds played a crucial role in the dissipation of energy during deformation. The dynamic oscillatory frequency sweep measurements of all samples were performed for the frequency range from 0.1 to 100rad s^{-1}, and G' and G'' are shown in Fig. 4b. G' was larger than G'' within the studied frequency range for all the TOCNF-CNTs/PAA hydrogels and the elastic character was the dominant factor, thereby exhibiting a typical gel-like character (Gao et al. 2016b). Moreover, G' increased significantly after the introduction of the TOCNFs and CNTs to the hydrogel network, demonstrating that the TOCNFs and CNTs enabled crosslinking hydrogel could maintain a stable network structure and transmit increased elasticity (Zhong et al. 2016). The G' value of the TOCNF-CNTs/PAA hydrogel

increased with the increase in the CNTs content, indicating that the crosslinking density of the network was enhanced. G'' of all the samples exhibited a clear dependency on the angular frequency. Both the G' and G'' of the hydrogels was greatest when the CNTs content was 0.7wt%. Notably, the crossover of G' and G'' for TOCNF-CNTs/PAA-0.7 took less time than that of the TOCNF/PAA and PAA (Fig. 4c), indicating a longer relaxation time (τ^*). A previous study reported that a longer τ^* corresponds to higher activation energy required for the breakage of cross-links (Zheng et al. 2020), thus, the TOCNF-CNTs/PAA hydrogel had a more stable framework. The plot of complex modulus (G^*), as a function of ω, displays a sharp contrast within these hydrogels (Fig. 4d). Besides, the TOCNF-CNTs/PAA possessed a higher G^* within the whole ω range, especially TOCNF-CNTs/PAA-0.7, which further confirmed that the CNTs enhanced the elasticity of the PAA hydrogel and the best enhancement effect was achieved when the content of the CNTs was 0.7wt%.

Mechanical performance

The as-prepared TOCNF-CNTs/PAA hydrogel exhibited excellent stretchability and mechanical properties. The hydrogel had a favorable capacity to withstand extensive deformations such as twisted stretching (Fig. 5a) and knotted stretching (Fig. 5b). Both compressive and tensile measurements were conducted to quantitatively analyze the mechanical properties of the hydrogels. Figure 5c displays the compressive stress-strain curves. The PAA hydrogel exhibited relatively low compression stress of the only 0.43MPa, even though the compressive deformation reached 80%. However, the TOCNF/PAA hydrogel displayed significantly better compression properties than the pure PAA hydrogel (~ 1.49MPa at 80% compressive strain). The enhancement benefited from the uniform dispersion of the TOCNFs and ample hydrogen bonds, and coordination bonds between the PAA matrix and TOCNFs, thereby resulting in the chain entanglement and reinforcing the crosslinking networks. Furthermore, the compressive strength further increased with the addition of the CNTs, and the optimal compressive performance of the TOCNF-CNTs/PAA-0.7 hydrogel was observed, which showed the highest compression stress at 70% compressive strain (~ 1.80MPa). It was worth noting that these values were 3.46 and 10.59 times more than those of the TOCNF/PAA (~ 0.52MPa) and the PAA (~ 0.17MPa), respectively. It can be intuitively seen from the illustration in Fig. 5c that the TOCNF-CNTs /PAA-0.7 hydrogel could support about 31 times of its weight without clear deformation or damage. The decrease in the compression strength after a further increase in the CNTs concentration can be attributed to the aggregation and stress concentration of the CNTs (Šupová et al. 2011). This study also investigated the tensile properties (Fig. 5d and Table S2, Supporting Information). The obtained results indicated that the pure PAA hydrogel exhibited an extremely low tensile strength (~ 25.58kPa) and elongation at break (~ 795.3%). TOCNFs, as nanofillers, reinforced the tensile properties and ductility of the PAA hydrogel, and the tensile strength and breaking elongation increased to ~ 35.78kPa and ~ 1069.5%, respectively. Analogous to the compressive strength and rheological viscoelasticity, increasing the CNTs content from 0.3wt% to 0.7wt% increased the tensile strength of TOCNF-CNTs/PAA hydrogels from 37.9kPa to 59.16kPa. In addition, further improving the CNTs content to 1.0wt% decreased the tensile strength to 49.17kPa. However, the elongation at break of the TOCNF-CNTs/PAA hydrogel were lower when compared with the TOCNF/PAA hydrogel, which could be attributed to the increase in the interaction between the CNTs and PAA chains which prevented the mobility of PAA

chains, thereby leading to the decrease in stretchability of the TOCNF-CNTs/PAA hydrogel (Cai et al. 2020). Figure 5e displays the image of the TOCNF-CNTs/PAA-0.7 before and after stretching, which demonstrates a smooth surface and can further withstand stretching as much as 450% without breaking.

Self-healing mechanism and behavior of the TOCNF-CNTs/PAA hydrogel

The prepared hydrogels had favorable mechanical strength and excellent self-healing ability. The hydrogel sample was artificially bisected using a blade, and the two freshly cut surfaces were contacted with each other for 12 h without any other external intervention. The obtained results indicated that the fracture traces at the two adjacent sections of the hydrogel interface were almost completely disappeared, and no cracking was observed under stretching. The possible self-healing mechanism of the TOCNF-CNTs/PAA hydrogel is schematically explained in Fig. 6a. These capabilities were associated with the rapid self-healing ability of the dynamic and reversible feature of the ionic coordination interactions (COO^- and Fe^{3+}) and hydrogen bonds (PAA, TOCNFs, and CNTs) (Wang et al. 2018b). It was worth noting that the PAA chains, TOCNFs, and CNTs within this hydrogel system had abundant COO^-, which crosslinked with Fe^{3+} via supramolecular metal-ligand complexation. When the hydrogel was broken, the Fe^{3+} ions dynamic migrated towards the freshly cut interfaces and interacted with COO^- with the assistance of the mobility of the PAA chain segments, which led to the reassembly of the two halves (Shao et al. 2017). Therefore, reconstruction of the network configuration between the two cut-off samples at the PAA hydrogel interface was achieved at room temperature. Repair using the ionic reintegration mechanism enabled the hydrogel samples to regain their mechanical strength. Moreover, the healed hydrogel could bend or even fold without breaking, demonstrating a good self-healing ability (Fig. 6b). The self-healing ability of the samples was further quantitatively analyzed using tensile tests. The TOCNF-CNTs/PAA-0.7 hydrogel was chosen as the specimen due to its best comprehensive properties including rheological and mechanical performances. The stress-strain behavior of the original and self-healing hydrogel is contrasted in Fig. 6c. The tensile stress-strain curves of the healed hydrogels exhibited an analogous trend with the original samples, indicating their outstanding self-healing properties. Furthermore, the healing efficiency was a significant parameter for identifying the degree of self-healing, which reached 98.99%, 98.33%, and 98.36% for the PAA, TOCNF/PAA, and TOCNF-CNTs/PAA-0.7 hydrogels, respectively (Fig. 6d). These phenomena proved that the hydrogels had a favorable self-healing ability and were almost completely healed insufficient time. Furthermore, the addition of the TOCNFs and CNTs had no significant impact on healing efficiency while improving the strength of hydrogels. However, the mechanical properties of the hydrogels could not be restored to 100% because the chemical crosslinking of the hydrogels was irreversible. Figure 6e displays the tensile stress-strain profiles of the TOCNF-CNTs/PAA-0.7 hydrogel for different healing times. The results indicated that as the healing time prolonged, the elongation at break was enhanced accordingly. For instance, the elongation at break reached ~ 300.2%, 542.7%, 679.4%, 823.3%, and 840.6% of the original elongation after healing for 2, 4, 8, 12, and 24 h, respectively. Figure 6f shows the healing efficiency of the TOCNF-CNTs/PAA-0.7 hydrogel for various healing times. In particular, the efficiency value of the TOCNF-CNTs/PAA-0.7 hydrogel achieved 35.01%, 63.82%, 79.39%, 96.37%, and 98.36% strain following the

periods of 2, 4, 8, 12, and 24 h, respectively. We concluded that the self-healing properties were improved with the extension of the healing time. Therefore, this extraordinary self-healing performance can enable these TOCNF-CNTs/PAA hydrogels to fulfill the demanding mechanical requirements.

Electrical conductivity of the TOCNF-CNTs/PAA hydrogel

The introduction of the CNTs components improved the rheological properties and mechanical performances of the hydrogels and achieved the controllable variation in the electrical conductivities (Fig. 7a). The electrical conductivity of the hydrogels without CNTs was approximately 2.3 S m^{-1}, which benefited from the presence of Fe^{3+} that could swiftly transport inside the hydrogel system (detailed data are presented in Table S3, Supporting Information). Furthermore, the electroconductivity of the composite hydrogels increased from 2.61 to 2.94 S m^{-1} with the increase in the CNTs content. The high luminance of a light-emitting diode (LED) vividly demonstrates the improvement of the conductivity of the composite hydrogels (inset of Fig. 7a). Enhancement of the conductivity of the composite hydrogels can be attributed to the good dispersion of the CNTs in the matrix-assisted by the TOCNFs, which was favorable for the development of conductive pathways under the conditions of extremely low content of CNTs (Dong et al. 2016). It was generally accepted that increasing the CNTs content led to more overlap between the CNTs, thereby resulting in better conductive pathways. However, when the content of CNTs increased to 1.0wt%, there were not enough TOCNFs to assist their dispersion, and the accumulation of redundant CNTs resulted in stress concentration and incomplete integration of the conductive network. Eventually, the conductivity only increased slightly for the composite hydrogels, while the mechanical strength and viscoelasticity were reduced. Furthermore, the conductivity of the TOCNF-CNTs/PAA-0.7 sample was tested under various cutting/healing cycles to discuss the electrical self-healing ability. The obtained *I-t* curve was recorded in Fig. 7b. After energization, the hydrogel exhibited a stable electrical conductivity in the curve as a smooth straight line. In addition, the current value became zero once the hydrogel was divided and the circuit was broken. The current than almost instantaneously returned to the initial value when the broken hydrogel was brought in contact. Interestingly, the hydrogel still maintained good stability after six cycles and the current was not significantly reduced. Therefore, the hydrogels displayed excellent repeatable restoration of the electrical performance. This excellent electrical recovery was also confirmed through the LED image displayed in Fig. 7c. The LED light successfully lit up when the circuit was connected, while the LED light turned off immediately after the light was cut. Besides, the LED light turned on again and still operated well once contact was achieved between the two cut samples.

Sensing performance of strain sensors assembled from TOCNF-CNTs/PAA

The TOCNF-CNTs/PAA hydrogel is a promising candidate for developing strain sensors because it has good mechanical flexibility, stretch-ability, self-healing ability, and conductivity. During the stretching process, the resistance change of the hydrogel exhibited a high sensitivity by converting mechanical deformation into detectable electrical signals for the strain sensing applications. The gauge factor (GF), the slope of the $\Delta R/R_0$-ε curve, was used to represent the sensitivity of the TOCNF-CNTs/PAA-0.7

hydrogel (Tan et al. 2020). When the maximum strain increased up to 400%, the corresponding GF increased from 0 to 6.86 (Figure S2a and b, Supporting Information). The GF value was higher than that of various similar hydrogels reported in previous literature, including PAAm-oxCNTs hydrogel (3.39 at 250–700%) (Sun et al. 2020), HPAAm/Cs-c-MWCNT hybrid hydrogel (3.2 at strains greater than 100%) (Xia et al. 2019) and PAA–rGO hydrogel (1.32 at 500%) (Jing et al. 2018). This implied that it can be used to generate the multifunctional strain sensors with a wide sensing range and considerable sensitivity, which enabled the as-prepared strain sensors to monitor human activities (Wang et al. 2018a). For instance, the TOCNF-CNTs/PAA-0.7 hydrogel was used to monitor the motion of finger knuckles (bending). The obtained results indicated that the current reduced gradually with the successive bending of the finger (Figure S2c), and the current returned to the original value when the finger was completely spread out. Meanwhile, the different motion amplitudes of the finger caused distinct current responses, implying excellent strain sensitivity. Moreover, the hydrogel still exhibited discernible strain sensitivity after 200 times (120° bending angle) repetition, implying decent repeatability of the strain sensor (Figure S2d).

Current research work has focused on electronic sensors that can recognize sign language (Eom et al. 2017; Gu et al. 2019; Guo et al. 2018). It is worth noting that traditional electronic sensors could detect simple finger bending, which is not appropriate for multi-dimensional sign recognition. The hydrogel-based electronic sensors developed in this study could not only display the ability to recognize simple articular up or down bending (Fig. 8a-d) but could also detect complex dimensional motions. For instance, three diacritical current amplitudes of upward and downward peaks were detected when someone wrote the letter A on paper, which completely differred from the current change of bending motions. Therefore, the TOCNF-CNTs/PAA hydrogel-based sensor qualified for explicitly distinguishing complex dimensional motions, which was beneficial for applications in the recognition of sign language. Besides, different electrical signals, which were characteristic and repeatable signals, were displayed when someone wrote different letters on the paper (such as ABCD) (Fig. 8e). Consequently, an as-prepared sensor could identify manual digital movements explicitly with dimensional movement resolution capability, which had tremendous significance for assisting the communication between deaf and mute people. Furthermore, the hydrogel was taped on the forehead, side face, chin positions, and larynx to investigate the sensitivity and reliability of the as-prepared sensor for minute facial expression detection (Fig. 8f-i). The obtained results indicated that each peak pattern matched a facial motion, which resulted from the signal variation in the current. It is important to note that facial emotions were controlled by several facial nerves and muscles, which were complicated and indistinguishable. However, the developed sensors still possessed the capacity to discern different types of facial muscle movement by mirroring distinct peak patterns of the current tendency (Xu et al. 2019). The repeatable peak patterns were also highly consistent with the original under the same motion detection, demonstrating high reliability and good stability of the as-developed sensors.

Conclusions

In summary, this study reported TOCNF-CNTs/PAA hydrogels based on physicochemical dual crosslinking and were highly viscoelastic, stretchable, conductive, and self-healing. Besides, the reported hydrogels had combined synergistic effects of hydrogen bonding, ionic coordination interactions, and polymer chain entangling. The incorporation of TOCNFs improved the mechanical strength of the PAA matrix. TOCNFs served as dispersing agents and benefitted the homogeneous dispersion of CNTs in the PAA matrix. TOCNF-CNTs complexes significantly reinforced the hydrogel network as well as imparted high conductivity to the hydrogels. The highly sensitive strain-sensor assembled by TOCNF-CNTs/PAA hydrogel can monitor human bodily motion in real-time by converting mechanical deformation into detectable electrical signals. This work provided a fundamental strategy to enhance the mechanical properties and conductivity of self-healing hydrogels via the incorporation of sustainable, renewable, and biodegradable TOCNFs and other highly conductive materials. The developed hydrogels were potential candidate materials for high-performance strain sensors and wearable devices.

Declarations

Acknowledgements

This work was funded by National Natural Science Foundation of China (31770609, 31901274), Natural Science Foundation of Jiangsu Province for Outstanding Young Scholars (BK20180090), Qing Lan Project of Jiangsu Province (2019), 333 Project Foundation of Jiangsu Province (BRA2018337), 13th China Special Postdoctoral Science Foundation (2020T130303), China Postdoctoral Science Foundation (2019M661854), Postdoctoral Science Foundation of Jiangsu Province (2019K142), Priority Academic Program Development (PAPD), and Analysis and Test Center of Nanjing Forestry University.

Data availability

The data that support the findings of this study are available from the corresponding author upon reasonable request.

References

Alias SA, Mhd Sarbon N (2019) Rheological, physical, and mechanical properties of chicken skin gelatin films incorporated with potato starch. NPJ Sci Food 3:26

Anjum S, Gurave P, Badiger MV, Torris A, Tiwari N, Gupta B (2017) Design and development of trivalent aluminum ions induced self-healing polyacrylic acid novel hydrogels. Polymer 126:196-205

Cai Y et al. (2020) Mixed-dimensional MXene-hydrogel heterostructures for electronic skin sensors with ultrabroad working range. Sci Adv 6: eabb5367

Chen Y et al. (2019) A Skin-Inspired Stretchable, Self-Healing and Electro-Conductive Hydrogel with A Synergistic Triple Network for Wearable Strain Sensors Applied in Human-Motion Detection.

Nanomaterials 9:1737

Dai S, Wang S, Yan H, Xu J, Hu H, Ding J, Yuan N (2019) Stretchable and self-healable hydrogel-based capacitance pressure and strain sensor for electronic skin systems. Mater Res Express 6:0850b0859

Dong B, Wu S, Zhang L, Wu Y (2016) High Performance Natural Rubber Composites with Well-Organized Interconnected Graphene Networks for Strain-Sensing Application. Ind Eng Chem Res 55:4919-4929

Dong K et al. (2018) A Stretchable Yarn Embedded Triboelectric Nanogenerator as Electronic Skin for Biomechanical Energy Harvesting and Multifunctional Pressure Sensing. Adv Mater 30:1804944

Eom J et al. (2017) Highly Sensitive Textile Strain Sensors and Wireless User-Interface Devices Using All-Polymeric Conducting Fibers. ACS Appl Mater Interfaces 9:10190-10197

Fujisawa S, Ikeuchi T, Takeuchi M, Saito T, Isogai A (2012) Superior reinforcement effect of TEMPO-oxidized cellulose nanofibrils in polystyrene matrix: optical, thermal, and mechanical studies. Biomacromolecules 13:2188-2194

Gao B et al. (2016a) Effect of a multiscale reinforcement by carbon fiber surface treatment with graphene oxide/carbon nanotubes on the mechanical properties of reinforced carbon/carbon composites. Compos Part A-Appl S 90:433-440

Gao F, Zhang Y, Li Y, Xu B, Cao Z, Liu W (2016b) Sea Cucumber-Inspired Autolytic Hydrogels Exhibiting Tunable High Mechanical Performances, Repairability, and Reusability. ACS Appl Mater Interfaces 8:8956-8966

Gu G, Xu H, Peng S, Li L, Chen S, Lu T, Guo X (2019) Integrated Soft Ionotronic Skin with Stretchable and Transparent Hydrogel-Elastomer Ionic Sensors for Hand-Motion Monitoring. Soft robotics 6:368-376

Guo Q, Luo Y, Liu J, Zhang X, Lu C (2018) A well-organized graphene nanostructure for versatile strain-sensing application constructed by a covalently bonded graphene/rubber interface. J Mater Chem C 6:2139-2147

Guo Y, Zhou X, Tang Q, Bao H, Wang G, Saha P (2016) A self-healable and easily recyclable supramolecular hydrogel electrolyte for flexible supercapacitors. J Mater Chem A 4:8769-8776

Han J, Lu K, Yue Y, Mei C, Huang C, Wu Q, Xu X (2019) Nanocellulose-templated assembly of polyaniline in natural rubber-based hybrid elastomers toward flexible electronic conductors. Ind Crop Prod 128:94-107

Han J et al (2019) A self-healable and highly flexible supercapacitor integrated by dynamically cross-linked electro-conductive hydrogels based on nanocellulose-templated carbon nanotubes embedded in a viscoelastic polymer network. Carbon 149:1–18

Hu S et al. (2019) Elastomeric conductive hybrid hydrogels with continuous conductive networks. J Mater Chem B 7:2389-2397

Huang Y et al. (2015) A self-healable and highly stretchable supercapacitor based on a dual crosslinked polyelectrolyte. Nat commun 6:10310

Isogai A, Saito T, Fukuzumi H (2011) TEMPO-oxidized cellulose nanofibers. Nanoscale 3:71-85

Jing X, Mi H-Y, Peng X-F, Turng L-S (2018) Biocompatible, self-healing, highly stretchable polyacrylic acid/reduced graphene oxide nanocomposite hydrogel sensors via mussel-inspired chemistry. Carbon 136:63-72

Koga H, Saito T, Kitaoka T, Nogi M, Suganuma K, Isogai A (2013) Transparent, conductive, and printable composites consisting of TEMPO-oxidized nanocellulose and carbon nanotube. Biomacromolecules 14:1160-1165

Krause B, Mende M, Pötschke P, Petzold G (2010) Dispersability and particle size distribution of CNTs in an aqueous surfactant dispersion as a function of ultrasonic treatment time. Carbon 48:2746-2754

Kumar P, Maiti UN, Lee KE, Kim SO (2014) Rheological properties of graphene oxide liquid crystal. Carbon 80:453-461

Li T, Li Y, Zhang T (2019) Materials, Structures, and Functions for Flexible and Stretchable Biomimetic Sensors. Accounts Chem Res 52:288-296

Liu S, Li K, Hussain I, Oderinde O, Yao F, Zhang J, Fu G (2018a) A Conductive Self-Healing Double Network Hydrogel with Toughness and Force Sensitivity. Chem-Eur J 24:6632-6638

Liu S, Oderinde O, Hussain I, Yao F, Fu G (2018b) Dual ionic cross-linked double network hydrogel with self-healing, conductive, and force sensitive properties. Polymer 144:111-120

Liu Y, He K, Chen G, Leow WR, Chen X (2017) Nature-Inspired Structural Materials for Flexible Electronic Devices. Chem Rev 117:12893-12941

Lu S et al. (2018) Diallyl dimethyl ammonium chloride-grafted cellulose filter membrane via ATRP for selective removal of anionic dye. Cellulose 25:7261-7275

Ma P-C, Siddiqui NA, Marom G, Kim J-K (2010) Dispersion and functionalization of carbon nanotubes for polymer-based nanocomposites: A review. Compos Part A-Appl S 41:1345-1367

Massoumi B, Jaymand M, Samadi R, Entezami AA (2014) In situ chemical oxidative graft polymerization of thiophene derivatives from multi-walled carbon nanotubes. J Polym Res 21:422

Olivier C, Moreau C, Bertoncini P, Bizot H, Chauvet O, Cathala B (2012) Cellulose nanocrystal-assisted dispersion of luminescent single-walled carbon nanotubes for layer-by-layer assembled hybrid thin films.

Langmuir 28:12463-12471

Saito T, Nishiyama Y, Putaux JL, Vignon M, Isogai A (2006) Homogeneous suspensions of individualized microfibrils from TEMPO-catalyzed oxidation of native cellulose. Biomacromolecules 7:1687-1691

Schwartz G, Tee BC, Mei J, Appleton AL, Kim DH, Wang H, Bao Z (2013) Flexible polymer transistors with high pressure sensitivity for application in electronic skin and health monitoring. Nat commun 4:1859

Shao C, Chang H, Wang M, Xu F, Yang J (2017) High-Strength, Tough, and Self-Healing Nanocomposite Physical Hydrogels Based on the Synergistic Effects of Dynamic Hydrogen Bond and Dual Coordination Bonds. ACS Appl Mater Interfaces 9:28305-28318

Sun X et al (2020) Carbon nanotubes reinforced hydrogel as flexible strain sensor with high stretchability and mechanically toughness. Chem Eng J 382:122832

Šupová M, Martynková GS, Barabaszová K (2011) Effect of Nanofillers Dispersion in Polymer Matrices: A Review. Sci Adv Mater 3:1-25

Tan X, Wang Y, Du W, Mu T (2020) Top-Down Extraction of Silk Protein Nanofibers by Natural Deep Eutectic Solvents and Application in Dispersion of Multiwalled Carbon Nanotubes for Wearable Sensing. ChemSusChem 13:321-327

Tang C, Zhou T, Yang J, Zhang Q, Chen F, Fu Q, Yang L (2011) Wet-grinding assisted ultrasonic dispersion of pristine multi-walled carbon nanotubes (MWCNTs) in chitosan solution. Colloid Surface B 86:189-197

Varga M et al. (2017) Diamond/carbon nanotube composites: Raman, FTIR and XPS spectroscopic studies. Carbon 111:54-61

Wan C, Jiao Y, Wei S, Zhang L, Wu Y, Li J (2019) Functional nanocomposites from sustainable regenerated cellulose aerogels: A review. Chem Eng J 359:459-475

Wan C, Li J (2016) Graphene oxide/cellulose aerogels nanocomposite: Preparation, pyrolysis, and application for electromagnetic interference shielding. Carbohydr polym 150:172-179

Wang T et al. (2018a) A Self-Healable, Highly Stretchable, and Solution Processable Conductive Polymer Composite for Ultrasensitive Strain and Pressure Sensing. Adv Funct Mater 28:1705551

Wang X, Dong L, Zhang H, Yu R, Pan C, Wang ZL (2015) Recent Progress in Electronic Skin. Adv Sci 2:1500169

Wang Y et al. (2018b) A novel design strategy for triple-network structure hydrogels with high-strength, tough and self-healing properties. Polymer 135:16-24

Wei Z et al. (2013) Autonomous self-healing of poly(acrylic acid) hydrogels induced by the migration of ferric ions. Polym Chem 4:4601

Xia S, Song S, Jia F, Gao G (2019) A flexible, adhesive and self-healable hydrogel-based wearable strain sensor for human motion and physiological signal monitoring. J Mater Chem B 7:4638-4648

Xu J, Wang G, Wu Y, Ren X, Gao G (2019) Ultrastretchable Wearable Strain and Pressure Sensors Based on Adhesive, Tough, and Self-healing Hydrogels for Human Motion Monitoring. ACS Appl Mater Interfaces 11:25613-25623

Yang J, Luo S, Zhou X, Li J, Fu J, Yang W, Wei D (2019a) Flexible, Tunable, and Ultrasensitive Capacitive Pressure Sensor with Microconformal Graphene Electrodes. ACS Appl Mater Interfaces 11:14997-15006

Yang JC, Mun J, Kwon SY, Park S, Bao Z, Park S (2019b) Electronic Skin: Recent Progress and Future Prospects for Skin-Attachable Devices for Health Monitoring, Robotics, and Prosthetics. Adv Mater 31:1904765

Yang W, Shao B, Liu T, Zhang Y, Huang R, Chen F, Fu Q (2018) Robust and Mechanically and Electrically Self-Healing Hydrogel for Efficient Electromagnetic Interference Shielding. ACS Appl Mater Interfaces 10:8245-8257

Yu H, Chen P, Chen W, Liu Y (2014) Effect of cellulose nanofibers on induced polymerization of aniline and formation of nanostructured conducting composite. Cellulose 21:1757-1767

Yue Y, Luo H, Han J, Chen Y, Jiang J (2020) Assessing the effects of cellulose-inorganic nanofillers on thermo/pH-dual responsive hydrogels. Appl Surf Sci 528:146961

Zhang T, Cheng Q, Ye D, Chang C (2017) Tunicate cellulose nanocrystals reinforced nanocomposite hydrogels comprised by hybrid cross-linked networks. Carbohydr Polym 169:139-148

Zheng C et al. (2020) A stretchable, self-healing conductive hydrogels based on nanocellulose supported graphene towards wearable monitoring of human motion. Carbohydr Polym 250:116905

Zhong M, Liu YT, Liu XY, Shi FK, Zhang LQ, Zhu MF, Xie XM (2016) Dually cross-linked single network poly(acrylic acid) hydrogels with superior mechanical properties and water absorbency. Soft Matter 12:5420-5428

Figures

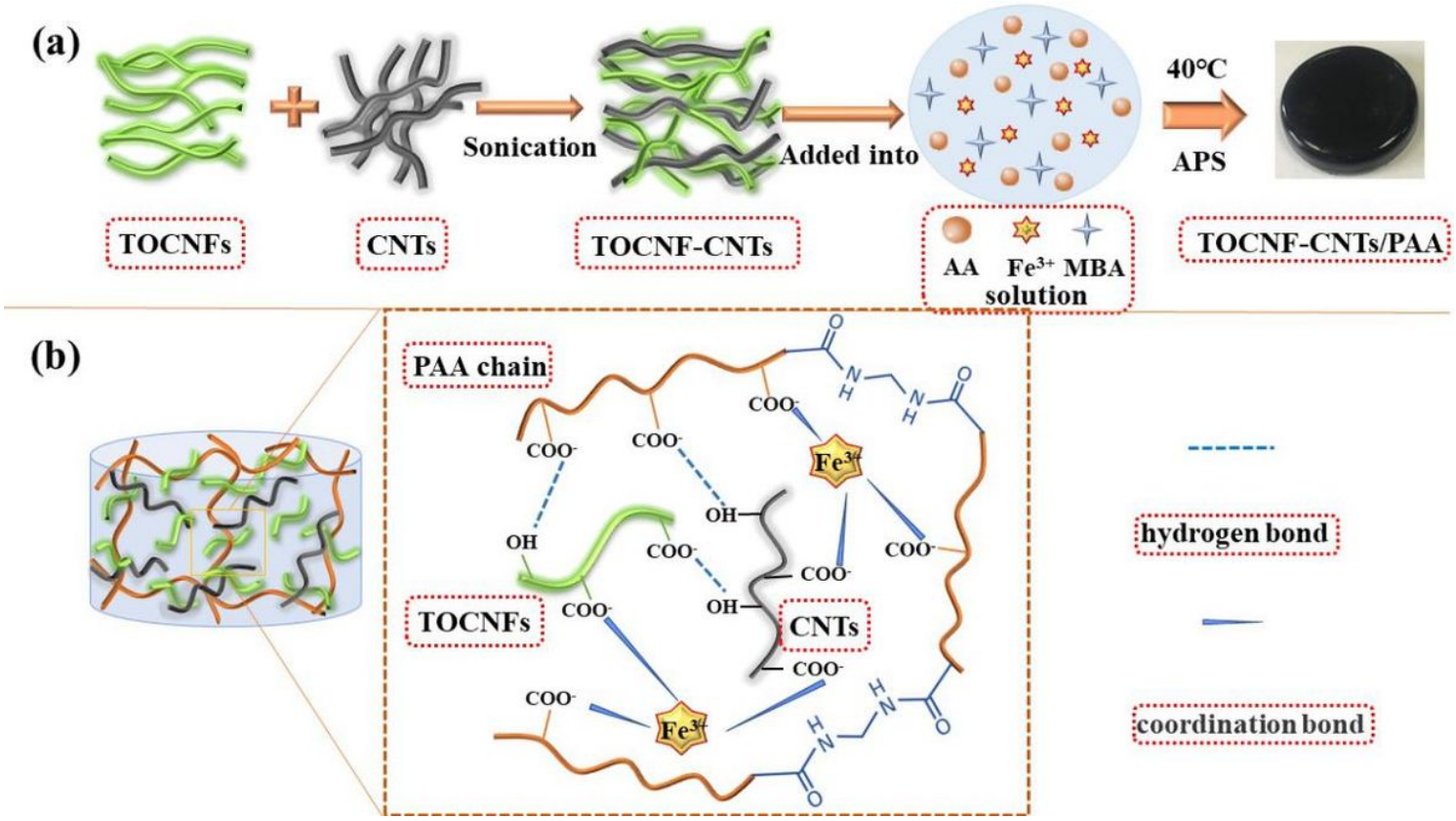

Figure 1

Preparation of TOCNF-CNTs/PAA. (a) Schematic illustration of the preparation process for hydrogels. (b) The formation mechanism of hydrogels

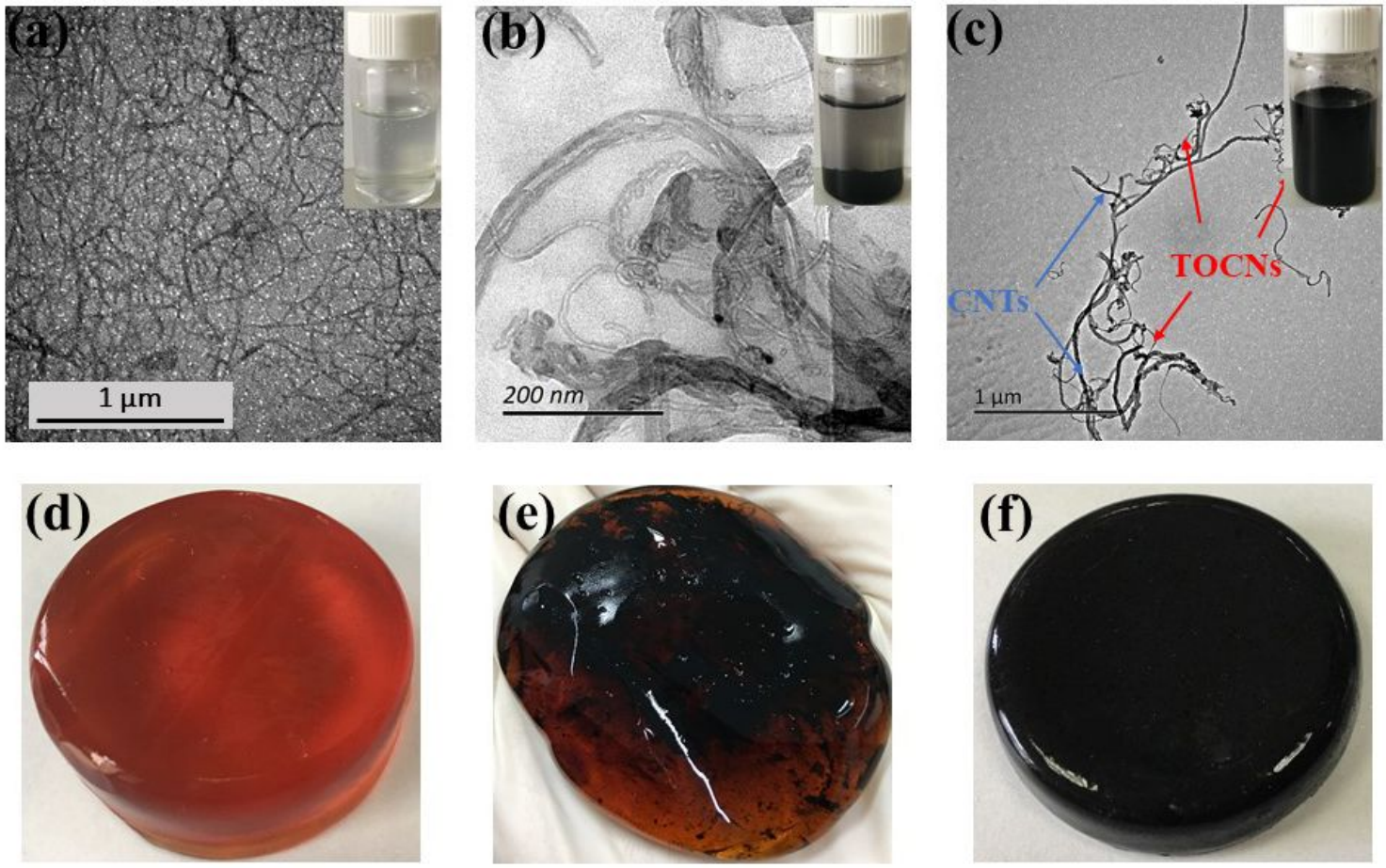

Figure 2

(a-c) TEM images and corresponding right insets show the dispersion of TOCNFs, CNTs, and TOCNF-CNTs nanohybrids, respectively. (d-e) Digital images of TOCNF/PAA, CNTs/PAA, and TOCNF-CNTs/PAA hydrogel, respectively

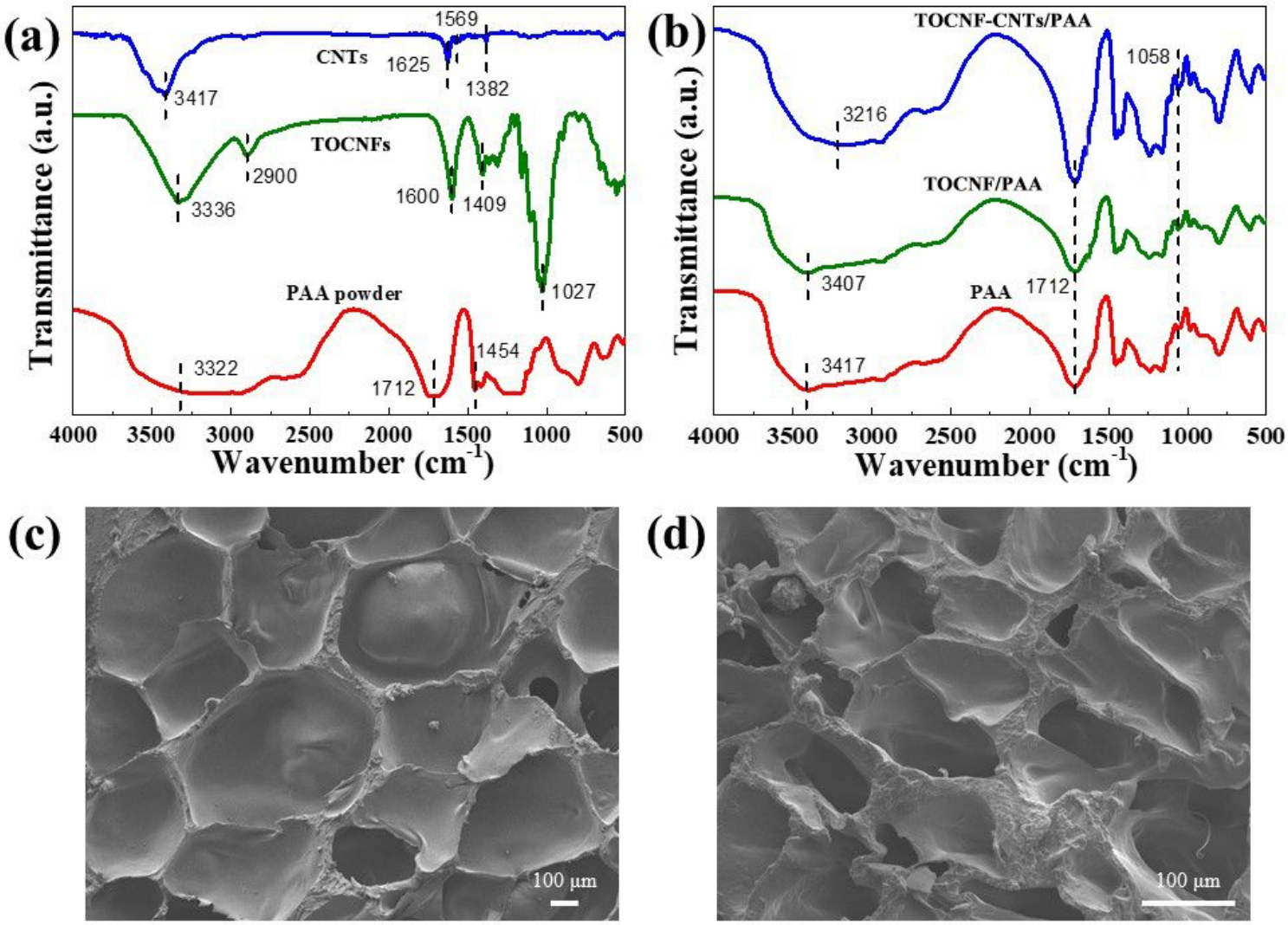

Figure 3

(a) FTIR spectra of pure PAA powder, CNTs, and TOCNFs; (b) FTIR spectra of PAA, TOCNF/PAA and TOCNF-CNTs/PAA hydrogel; SEM images of (c)TOCNF/PAA hydrogel and (d) TOCNF-CNTs/PAA hydrogel

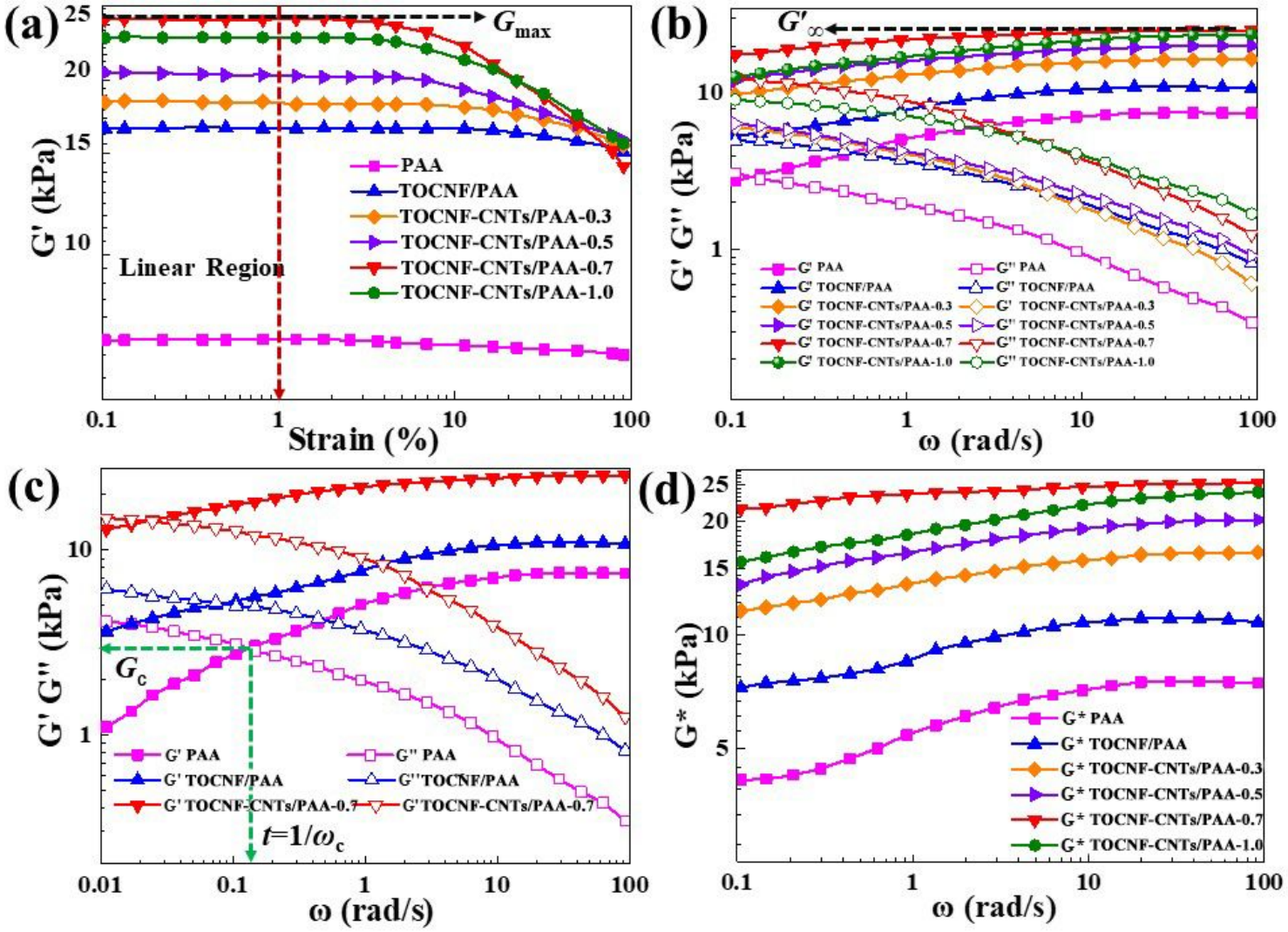

Figure 4

Dynamic viscoelasticity of hydrogels at 25 °C. (a) G' as a function of oscillatory strain amplitude (γ) (ω = 1.0 Hz). (b) G' and G" as a function of the frequency sweep test. (c) G' and G" as a function of frequency sweep test for PAA, TOCNF/PAA, and TOCNF-CNTs/PAA-0.7. (d) G* versus frequency

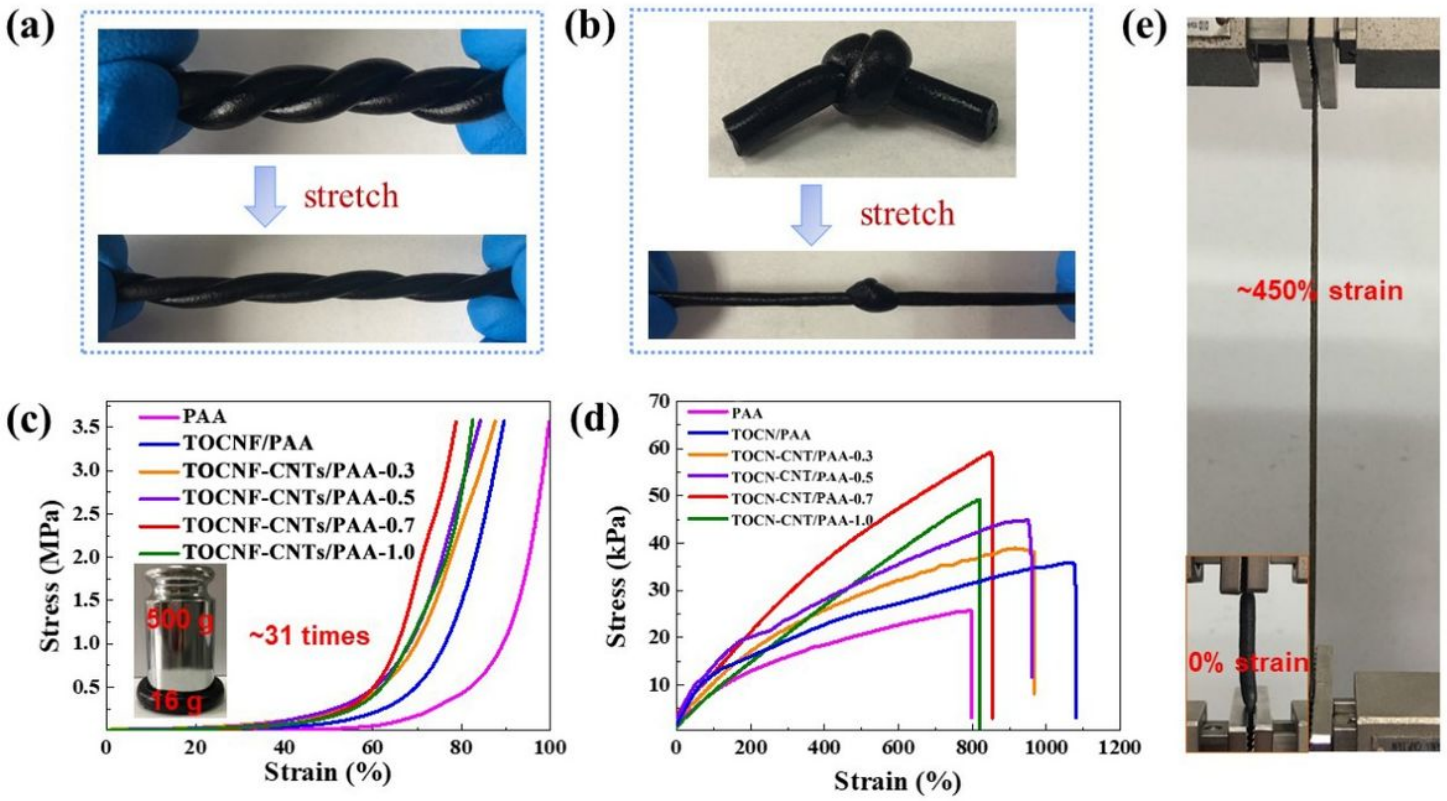

Figure 5

(a) and (b) Mechanical toughness under twisting and stretching of TOCNF-CNTs/PAA hydrogel. (c) Compressive stress-strain curves. (d) Tensile stress-strain curves. (e) Digital images of TOCNF-CNTs/PAA-0.7 hydrogel before and after stretching

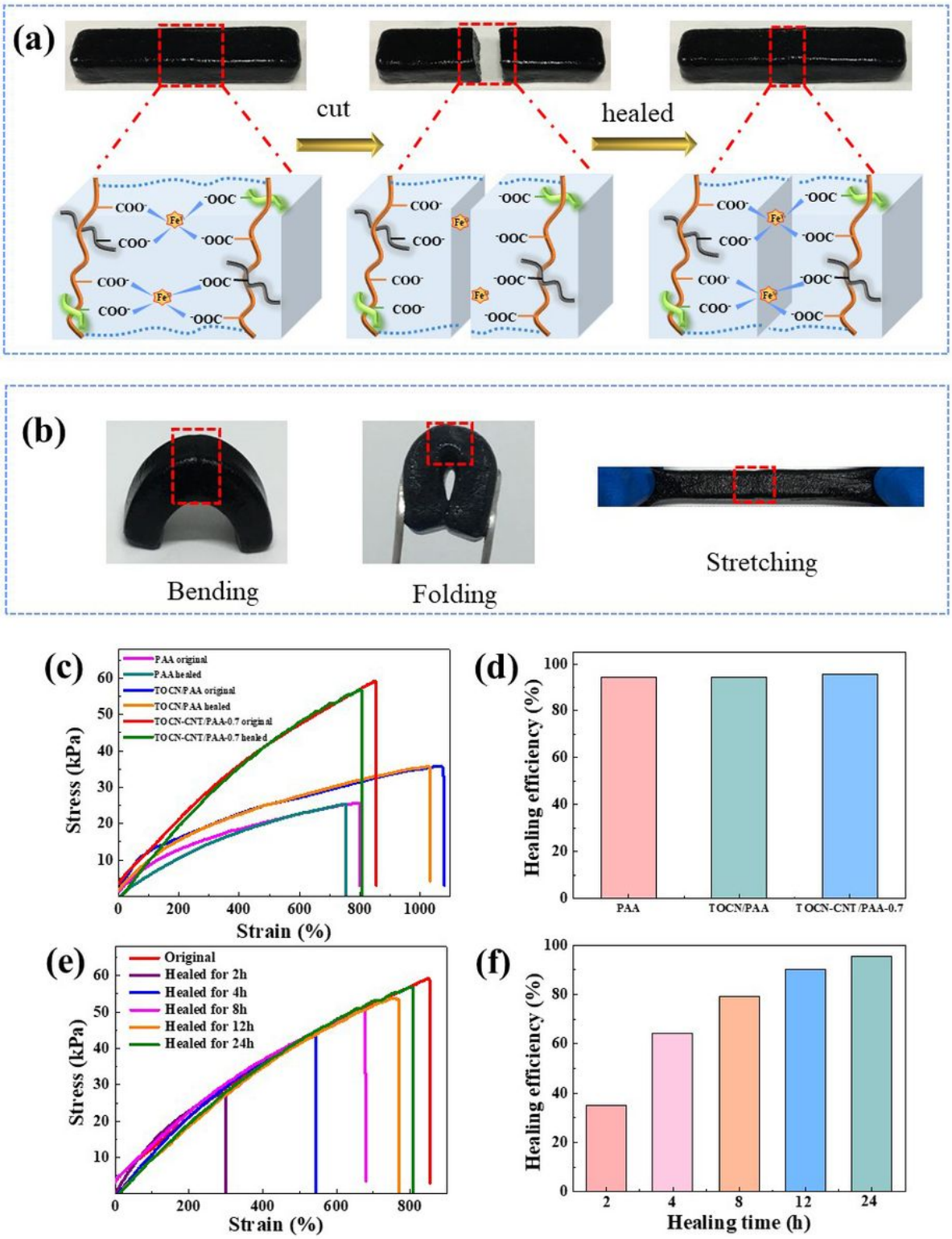

Figure 6

Self-healing properties of TOCNF-CNTs/PAA hydrogel. (a) Schematic illustration of the self-healing mechanism. (b) Self-healing behavior. (c) Tensile stress-strain curves and (d) corresponding healing efficiencies of the original and healed hydrogel with different components. (e) Tensile stress-strain curves and (f) corresponding healing efficiencies of TOCNF-CNTs/PAA-0.7 hydrogel at different times

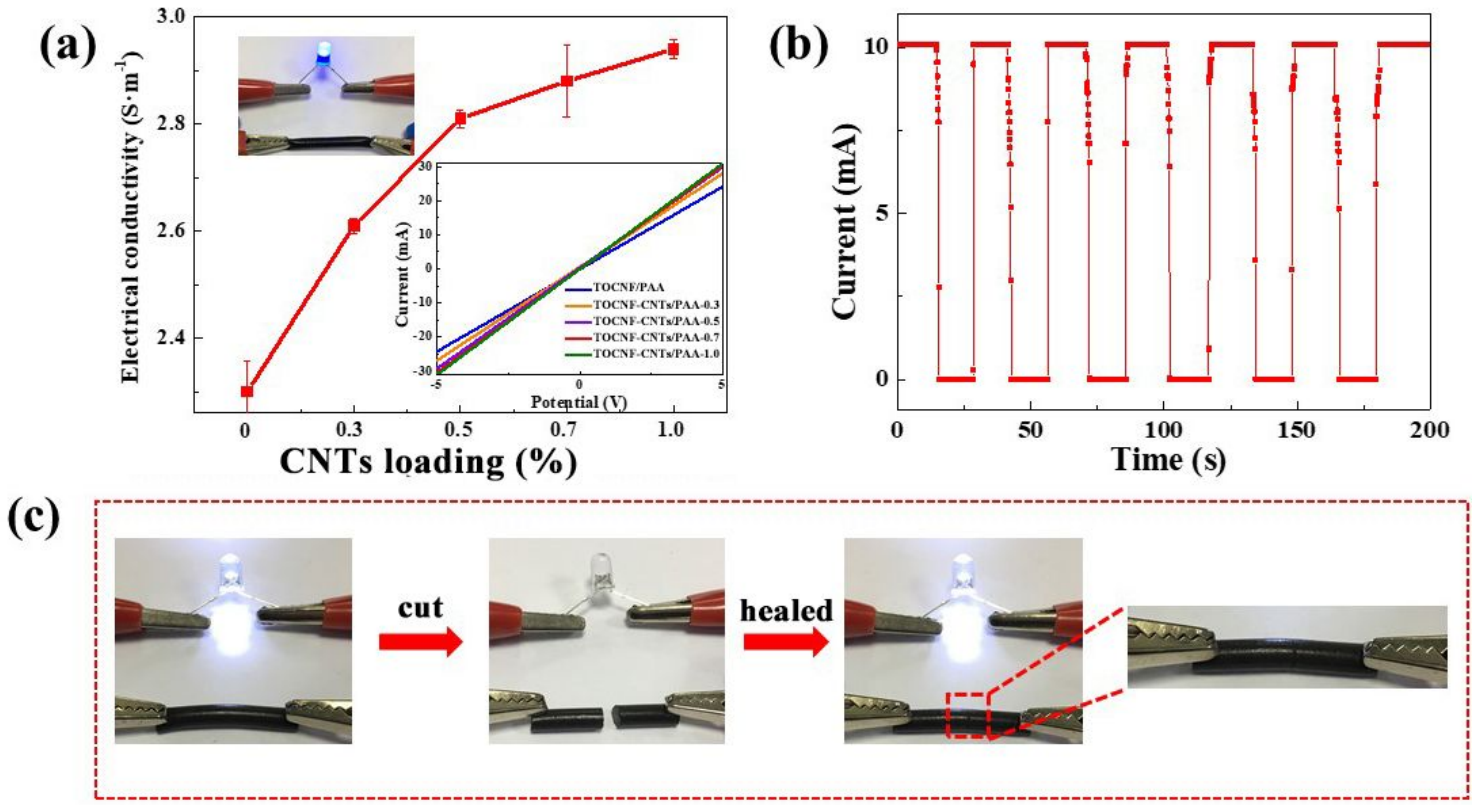

Figure 7

(a) Electrical conductivity of the prepared hydrogel. (b) I-t curve of TOCNF-CNTs/PAA-0.7 hydrogel under repeated cutting/healing cycles. (c) Demonstration of electrical self-healability of the hydrogel when connected to a circuit with LED light

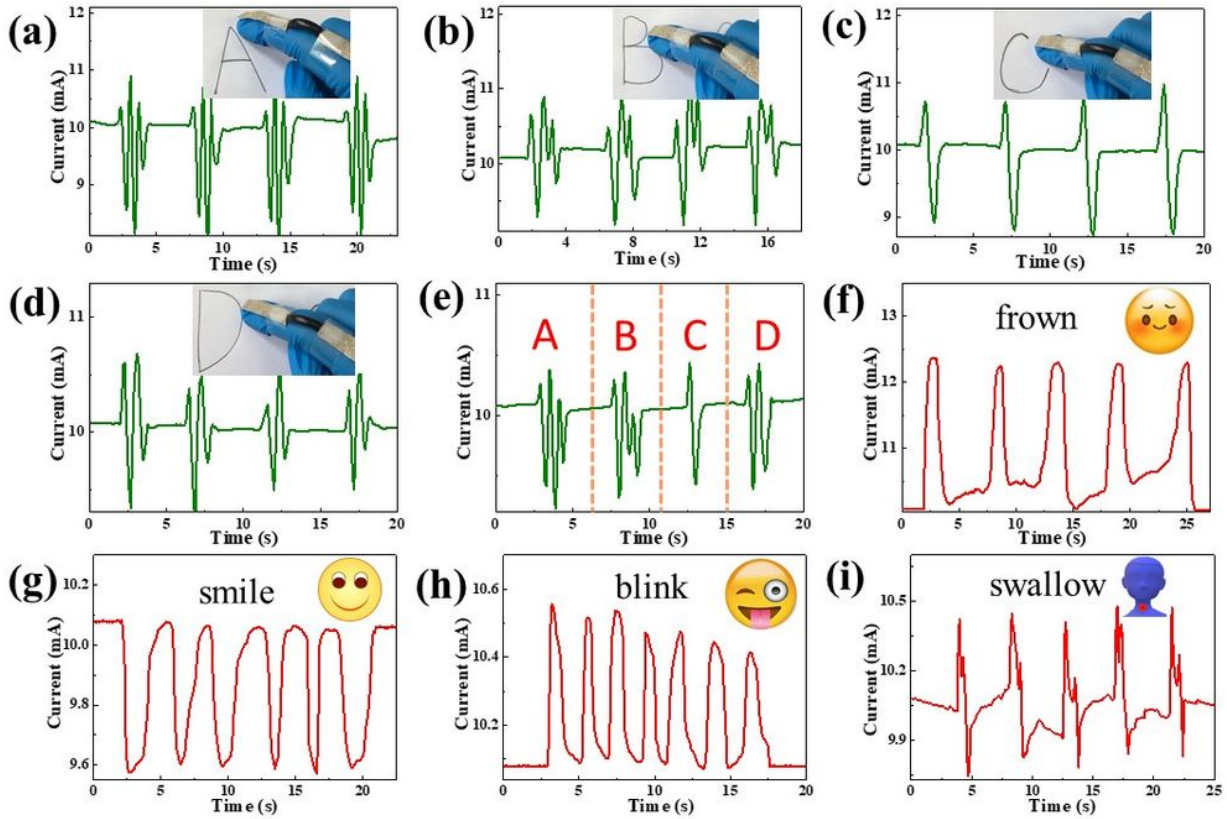

Figure 8

(a-e) Current variations of the sensor with volunteer writing on paper. Corresponding current signs of different motions: frown (f), smile (g), blink (h), and deglutition (i)

Supplementary Files

This is a list of supplementary files associated with this preprint. Click to download.

- TOC.png
- SupportingInformation.docx